Temperature Dependence of Förster Thermalization and Population Decay in PbSe Nanocrystals

ARTICLE *in* THE JOURNAL OF PHYSICAL CHEMISTRY C · DECEMBER 2013

Impact Factor: 4.77 · DOI: 10.1021/jp4109046

3 AUTHORS, INCLUDING:

Rafael Quintero-Torres
Universidad Nacional Autónoma de México
43 PUBLICATIONS **136** CITATIONS
SEE PROFILE

Frank C J M van Veggel
University of Victoria
120 PUBLICATIONS **6,848** CITATIONS
SEE PROFILE

THE JOURNAL OF PHYSICAL CHEMISTRY C

Article

pubs.acs.org/JPCC

Temperature Dependence of Förster Thermalization and Population Decay in PbSe Nanocrystals

Rafael Quintero-Torres,*[,†] Frank C. J. M. van Veggel,[‡] and Jeff F. Young[§]

[†]Departamento de Nanotecnología, Centro de Física Aplicada y Tecnología Avanzada, UNAM Campus Juriquilla, Boulevard Juriquilla 3001, Juriquilla Querétaro 76230, México

[‡]Department of Chemistry, University of Victoria, Victoria, British Columbia, Canada V8W 3 V6

[§]Department of Physics and Astronomy, Advanced Materials and Process Engineering Laboratory, University of British Columbia, Vancouver, British Columbia, Canada V7R 3Z6

ABSTRACT: Time-resolved photoluminescence spectroscopy is used to quantify the Förster-mediated exciton migration rate and the exciton population decay rate in drop-cast solid emulsions of PbSe colloidal nanocrystals emitting near 1.5 μm from 77 to 300 K. For both unimodal and bimodal emulsions, at a fixed temperature in a given sample the measured time constants that characterize the fast transient decay (blue side of the spectrum) and buildup (red side of the spectrum) vary considerably with emission wavelength, but the average fast time constant, ~25 ns, varies little (i.e., within <25%) with temperature from 77 to 300 K. Over the same temperature range, the exciton population lifetime, ascribed to nonradiative decay, decreases by ~5 times but is always longer than the Förster time constant. The increase of the Förster-mediated efficacy of exciton redistribution at low temperatures before they decay is therefore almost all due to the variation of the nonradiative decay rate. By analyzing the temporally resolved and steady-state emission spectra, it is noted that the time required for the exciton population to equilibrate is nonexponential and considerably longer (~150 ns) than the rapid decay and buildup time constants extracted from the decay curves at fixed wavelengths.

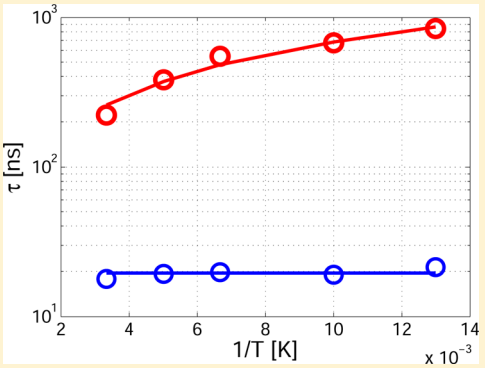

INTRODUCTION

Densely packed colloidal nanocrystal ensembles are of considerable interest for solar energy harvesting,[1,2] photodetectors,[3,4] and light-emitting diodes[5] due to the ease with which their bandgap energy can be tuned over a wide range and their relatively simple and inexpensive synthesis. Pb-based colloidal "nanospheres", most prominently PbSe or PbS with diameters in the range of 3.5−6 nm, are of particular interest at energies below the bandgap of silicon, down to <800 meV.

The distribution of particle sizes and hence bandgaps in solid-state emulsions formed by drop-casting nanocrystalline solutions is a minimum of ~4% for nominally monodispersed samples and can be controlled by blending different-sized monodispersed solutions before drop-casting. When above bandgap radiation is absorbed by any given particle within such a sample, it is usually assumed that rapid energy relaxation within the particles results in the formation of a "ground state" exciton within a few picoseconds. The subsequent fate of the excitons then depends strongly on the details of their environment. In dilute solutions, the excitons typically will either radiatively decay by emitting a photon or nonradiatively recombine via midgap and/or surface states in the particle where the exciton was first created. If free charges are trapped near a particle, efficient, nonradiative Auger recombination effectively excludes them when considering the dynamics of the ensemble's exciton population.

In densely packed, three-dimensional (3D) arrays of nanocrystals, it is well-known that the excitons can also move from one particle to another via the dipole−dipole, Förster interaction.[6,7] Because the Förster interaction is expected to depend on the inverse sixth power of the interparticle separation, the density and sizes of particles in the ensemble will determine whether or not there is significant equilibration of the as-excited exciton population within the ensemble of particles before radiative and/or nonradiative recombination occurs. Significant nonradiative transfer of excitons between particles before they decay may be advantageous for certain device applications.[8]

Time-resolved spectroscopy of the radiative emission from 3D emulsions and 2D arrays[9] of mono- and multidispersed colloidal nanocrystals excited by short-pulse lasers has been used by several groups to study their exciton dynamics.[10−14] Common to all of these reports is that the time-dependence of the emission from the blue side of the spectra contains a "fast component" that can be easily distinguished from a slower

Received: November 5, 2013
Revised: December 12, 2013
Published: December 16, 2013

   dx.doi.org/10.1021/jp4109046 | J. Phys. Chem. C 2014, 118, 1377−1385

component that is often similar for all wavelengths in the emission spectrum. The fast component, absent in dilute solutions of the same particles so long as the excitation level is sufficiently low, is evidence of exciton redistribution among the particles on time scales shorter than the population lifetime, which is associated with the slower decay.

The fast component has reasonably been attributed to the Förster interaction, and efforts to compare the fast decay rate with the theoretical expression for this process

$$k = \frac{1}{\tau_R}\left(\frac{|R|}{R_0}\right)^{-6} \quad (1)$$

where τ_R is the radiative lifetime with no energy transfer, R is the interparticle separation, and R_o is the "Förster radius" for a given pair of particles, have yielded estimated particle separations, R consistent with what one would expect for close-packed 3D arrays of the particles used in the experiments. The validity of this analysis is questionable to some extent given that the fast component of the reported decay curves typically varies considerably as a function of spectral position, and the R_o value also depends strongly on the relative sizes of the interacting particles. The latter is relevant because for a given emission frequency the originating, relatively small particle will be surrounded by particles of different sizes and hence R_o values.

Some of the other reported behavior is less consistent between particle types and laboratories. In some, but not all cases, there is a clear buildup time observed on the red side of the spectra. When this is present, the corresponding time constant is often not compared to the fast decay constant observed in the blue side of the spectra. In perhaps the most comprehensive analysis, done as a function of temperature using CdTe particles,[15] the authors argue that it is in fact this buildup time that should be attributed to the "Förster interaction rate". They then conclude that the Förster interaction rate is essentially temperature independent from 300 to 100 K and then decreases by an order of magnitude by 20 K. In another temperature dependent study, using PbS particles, the authors state that the Förster energy transfer rate, based on the fast component of the decay from the blue part of the spectra, increases from 1/50 ns^{-1} at 200 K to 1/30 ns^{-1} at 160 K. Unfortunately, the steady-state spectra from even the monodispersed samples used in both of those studies were quite complicated.

The time-resolved, temperature-dependent emission from high-quality PbSe nanocrystals reported here shares features reported by others, but there are distinguishing attributes. By analyzing the dynamics of several samples at multiple emission wavelengths and temperatures, we conclude that both the rates of the rapid rise on the red side and the rapid decay on the blue side of the spectra are wavelength dependent at a given temperature but that the average value of these rates shows no clear dependence on the temperature from 300 to 77 K.

The quantity that varies most over this temperature range, almost an order of magnitude, is rather the relatively slow exciton population decay rate. For low temperatures, more of the exciton population is redistributed via the Förster interaction before the population decays: the "Förster efficiency" is higher at lower temperatures almost exclusively because of the longer nonradiative recombination times, not a change in the "Förster scattering time". Higher Förster efficiency leads to more prominent PL buildup on the red side of the spectrum.

The time-dependent spectra are also analyzed to highlight and discuss the subtle but quantitatively significant difference between the fast "Förster scattering time" as extracted from exponential fits of the initial decay/buildup of the emission versus the "equilibration time" required for the excitons to establish a quasi-steady-state distribution among the available particles. Finally, a simple phenomenological model of the Förster interaction rate is offered to explain the measured, weak temperature dependence between 77 and 100 K.

SAMPLE PREPARATION AND EXPERIMENTAL PROCEDURES

All results described below were obtained using two batches of PbSe colloidal QDs prepared as described in ref 16−18 with nominal diameters of 4.0 nm (batch A) and 4.5 nm (batch B).[19] Drop-cast versions of the individual, unimodal A and B solutions and of a bimodal (nominally a 50/50 blend of A and B by weight) solution were formed in a nitrogen-filled glovebox on silicon substrates that were RCA-1 cleaned and immersed in a dilute buffered oxide etch solution for 1 min prior to QD treatment. Before deposition, QDs were evaporated from TCE under nitrogen flow, weighed, and dispersed in spectroscopic grade hexanes (Sigma Aldrich) to a concentration of 50 mg/mL for drop-casting. Substrates for drop-cast samples were first mounted in the cryostat, through which nitrogen flowed, and several <0.1 mL drops of the highly concentrated QD solution were pipetted onto the sample substrate to form a single, conglomerated opaque emulsion of QDs several square millimeters in area. Nitrogen flow was continued for several minutes to allow for residual solvent evaporation and finally the cryostat was put under vacuum. Submonolayer distributions of QDs were formulated inside a nitrogen-filled glovebox using a dip-coating procedure. Substrates were suspended (sample plane vertical), immersed into the QD solution at a speed of 1 mm/s, held for 5 s, withdrawn at a speed of 0.8 mm/s, and placed inside the cryostat. The cryostat, containing the dip-coated samples, was removed from the glovebox, and nitrogen flow through the sample chamber of the cryostat was quickly established and maintained until the sample was mounted, followed by evacuation of the sample chamber to $<10^{-3}$ Torr.

Both time-integrated spectra and spectrally integrated, time-resolved decay curves were used to compare various preparations. Steady state PL (SSPL) spectra were obtained using a CW HeNe laser, while time-resolved spectra (either spectrally integrated or filtered using 12 nm wide bandpass filters) were obtained using either an ∼1.5 ps pulsed Ti:sapphire laser (∼800 nm) operated at 80 MHz in conjunction with an electro-optic pulse-plucker or a variable repetition rate diode laser @ 658 nm with pulse duration ∼500 ps. The measured decay time constants were the same for either excitation source. In all cases, the excitation beam was directed by a reflective objective to a spot size on the sample of diameter ∼3 μm. In contrast to the dilute solutions, the SSPL spectra and the time-resolved decay curves obtained from the dense, randomly packed QDs in drop-cast films are very sensitive to the optical excitation rate. In order to obtain intensity-independent results, the average excitation intensity had to be kept below 0.1 MW/cm^2. The solid samples were mounted in an evacuated coldfinger cryostat, and the PL emission normal to the surface was collected with the same reflective objective and directed either to a Bruker Fourier

dx.doi.org/10.1021/jp4109046 | J. Phys. Chem. C 2014, 118, 1377−1385

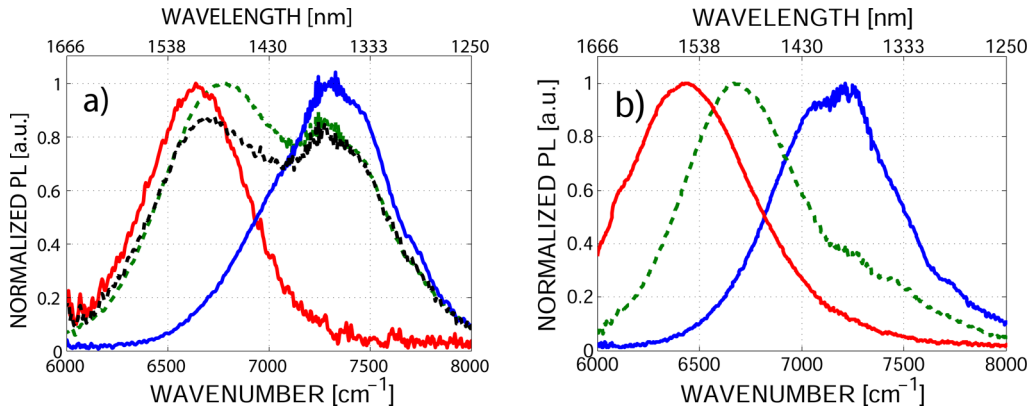

Figure 1. Normalized plots of steady state photoluminescence for two unimodal size distributions of quantum dots; solid red 4.5 nm diameter (sample B), blue 4.0 nm (sample A), and from a bimodal mixture of A and B (segmented green). (a) Panel is from the quantum dots in solution at 300 K and (b) is from solid state thick films at 300 K. The dotted curve in (a) is the equally weighted sum of the two unimodal spectra for comparison to the blend spectrum.

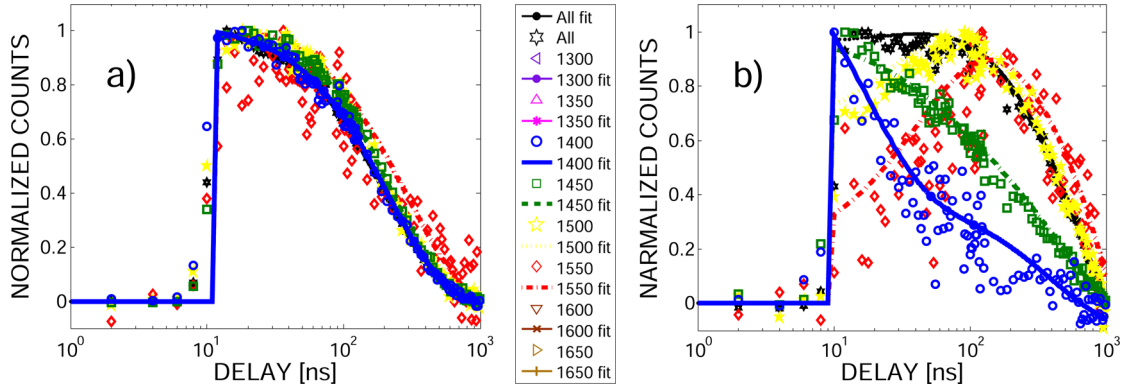

Figure 2. Normalized temporal evolution of the PL signal from a solid state formulation of sample A particles obtained at different wavelengths; 1400 nm (blue), 1450 nm (green), 1500 nm (yellow), 1550 nm (red), and spectrally integrated (black) at 300 K (a) and 77 K (b). The scatter in the data reflects the uncertainty of the raw measurements. The solid lines are best fits assuming an instantaneous initial excitation followed by a subsequent evolution described by two exponentials (see text).

Transform spectrometer for time integrated spectra or an InGaAs infrared single photon detector for spectrally integrated, time-resolved measurements. The synchronization and time delay control was achieved with two pulse generators, and a long wave pass filter was used to ensure only the PL was detected in the fast detector.

RESULTS WITH STEADY-STATE EMISSION SPECTRA

Figure 1a shows three steady-state PL (SSPL) spectra corresponding to dilute unimodal solutions of sample A and sample B individually and the bimodal blend at 300 K. The fact that the SSPL spectrum from the blend is essentially a linear superposition of the two individual spectra (see the dotted curve in Figure 1a) suggests that there is negligible interaction of excitons between the two species when in dilute solution.

Figure 1b shows the corresponding SSPL spectra from all three samples in drop-cast form, again at 300 K. All are red shifted with respect to the corresponding solution spectra, and the blend spectrum from the drop-cast sample is much more heavily weighted in favor of the larger, lower energy QDs. This is qualitatively consistent with a scenario wherein excitons in closely spaced QDs can migrate via the Förster interaction and thus explore the available density of states (DOS) as defined by the size distribution of the ensemble. The solution spectra provide a measure of the DOS (within some Stokes shift), and the drop-cast spectra represent the redistribution of the excitons within that DOS (again within a Stokes shift, which could be different from the Stokes shift in solution). If there was no differential Stokes shift between solution and the drop-cast formulations, the redshifts of the monodispersed spectra would provide a measure of the effective temperature describing the exciton distribution within the QD ensemble; the cooler the effective temperature, the larger the redshift. This qualitative picture for the shift is difficult to quantify because of the unknown differential Stokes shift, and the fact that the actual DOS associated with the distribution of QD sizes is considerably narrower than the solution PL line width would indicate, because the solution line width involves a convolution of the homogeneous line width of individual QD emission with the DOS distribution.[22]

In the case of the blend spectra, there is addition information associated with the difference in the relative contributions of the small and large QDs on going from solution to drop-cast formulations. Again, the observed behavior is qualitatively consistent with thermalization of the distribution in drop-cast samples, as there is clearly less contribution from the smaller, higher energy QDs than in solution. However, again, quantitative evaluation based on the SSPL spectra is not possible, owing to the same factors identified above, together

dx.doi.org/10.1021/jp4109046 | J. Phys. Chem. C 2014, 118, 1377−1385

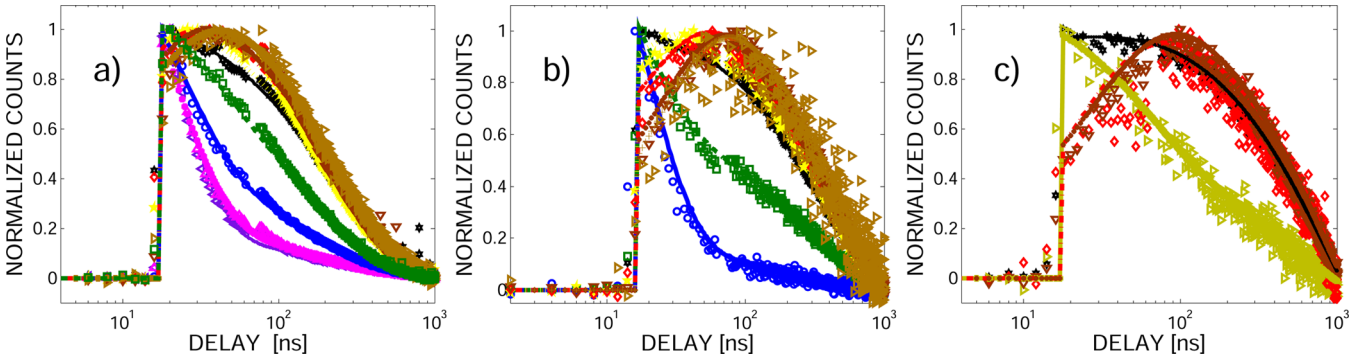

Figure 3. Normalized temporal evolution of the PL signal from a solid state formulation of the blend of sample A and B particles obtained at different wavelengths; 1300 nm (pink), 1350 nm (purple), 1400 nm (blue), 1450 nm (green), 1500 nm (yellow), 1550 nm (red), 1600 nm (brown), and 1650 nm (gold), and spectrally integrated (black) at 300 K (a), 200 K (b), and 77 K (c). The scatter in the data reflects the uncertainty of the raw measurements. The solid lines are best fits assuming an instantaneous initial excitation followed by a subsequent evolution described by two exponentials (see text).

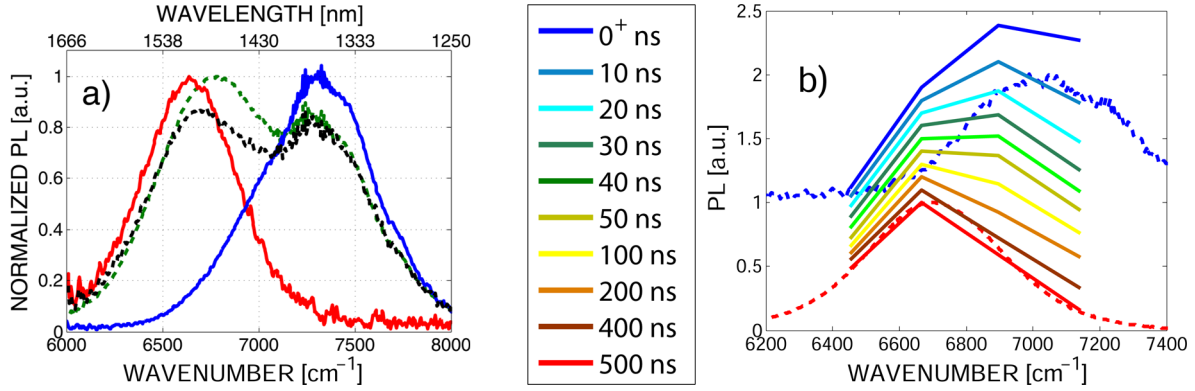

Figure 4. Energy dependence of the emission spectra at different times after excitation for the bimodal blend of A and B in solid form at 300 K (a) and for the unimodal sample A at 77 K (b). The legend describes the times at which the spectra are displayed. In (a), the red dashed line represents the SSPL spectrum from the same sample at 300 K while the blue dashed curve is the SSPL spectrum from the blend in solution. In (b), the dashed red curve is the SSPL spectrum from the same sample at 77 K and the broken blue curve is the SSPL spectrum from a dilute monolayer made from a solution of sample A at 77 K. The spectra at different times were normalized to the signal at 6250 cm^{-1} (a), and 6666 cm^{-1} (b) and shifted for clarity.

with the fact that the relative weighting depends both on the energy separation of the two peaks in the DOS for the blend, and their inhomogeneous linewidths. These challenges in quantitatively extracting thermalization information from the SSPL spectra motivate the time-dependent studies described below.

RESULTS WITH TRANSIENT DECAY

Figure 2 shows the time-resolved PL (TDPL) curves obtained from the unimodal solid state formulation of sample A at both 300 and 77 K. At 300 K, there is very little variation in the decay dynamics at different wavelengths. In contrast, there is a strong spectral dependence at 77 K with the blue side clearly showing a relatively fast decay and the red side a relatively fast buildup.

Figure 3 shows the TDPL obtained from drop-cast film made from the blend of batches A and B at 300, 200, and 77 K. Clearly there is strong spectral dependence to the decay curves at all three temperatures, each exhibiting a relatively fast decay component on the blue side and a corresponding fast buildup component on the red side.

Another way to display these dynamics is to plot the spectrally sampled spectra at various times after laser excitation. Figure 4 does this for the bimodal blended sample at 300 K and the unimodal sample A at 77 K.

DISCUSSION

All of these results are qualitatively similar to previously reported studies of different types of colloidal nanocrystals.[20] However, one main difference is that most others report a greater spectral dependence and clear evidence of a fast decay component on the blue side of the spectra from unimodal solid state samples even at room temperature. We attribute this to the fact that the data in Figure 2 was obtained using very low excitation powers in comparison to those reported by others: we observe more spectral dependence and the emergence of more significant fast transients from unimodal samples excited by higher power pulses.

Much of the related literature analyzes the transient decay curves to extract a fast "Förster time constant", and a slower population decay time constant. The former is often used to extract a mean Förster radius for the particles (R_0 in eq 1), assuming one knows the average interparticle separation (R in eq 1)[10] or to compare the mean interparticle separation one gets from eq 1 with the particle radius, assuming one can estimate the Förster radius.[11] When data over a range of temperatures has been measured, the ratio of fast and slow time constants is attributed to a temperature dependent "Förster efficiency", which nominally provides a measure of the extent of equilibration that occurs among the particles before the excitons recombine, either radiatively or nonradiatively.

dx.doi.org/10.1021/jp4109046 | J. Phys. Chem. C 2014, 118, 1377−1385

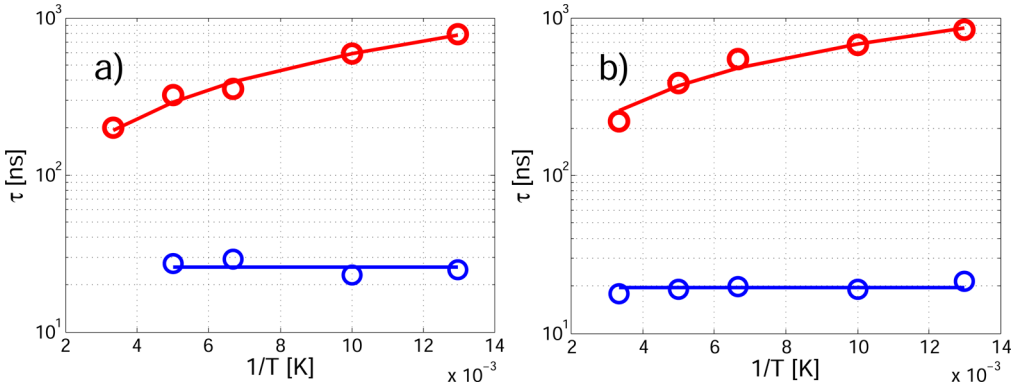

Figure 5. The fast (blue) and slow (red) time constants extracted from the TDPL curves using eq 3 as a function of inverse temperature for the unimodal sample B (a) and the bimodal mixture of A and B (b). The lines are guides to the eye for the temperature dependence of the average values and the estimated uncertainties in the time constant are consistent with the symbol size. The uncertainty in the inverse temperature is negligible for estimating the trend lines.

While these are reasonable ways to simply parametrize a complex system's dynamical behavior, they typically ignore two significant facts; (i) the fast decay and fast buildup time constants typically depend significantly on wavelength, and perhaps more significant (ii) the time for the spectra to fully develop a quasi-steady-state shape is typically significantly longer than the fast time constant extracted and used as a measure of the "Förster time constant".

Below, we analyze and interpret our data based on the following picture for exciton dynamics in these solid emulsions, given that the theoretical Förster transfer rate, k, from a single donor to a single acceptor separated by a distance R, is related to the donor's emission spectrum, $F_1(\nu)$, and the acceptor's molar extinction coefficient, $\varepsilon_2(\nu)$, as[11]

$$k = \left(\frac{9000\ln(10)\kappa^2 c^4}{128\pi^5 n^4 N_A \tau_R}\right)|\vec{R}|^{-6}\frac{\int F_1(\nu)\varepsilon_2(\nu)\nu^{-4}\,d\nu}{\int F_1(\nu)\,d\nu} \quad (2)$$

where $\kappa^2 = \langle\cos\theta - \cos\alpha\cos\beta\rangle$, where θ is the angle between the two involved dipoles from the observation point; α and β are the angles that the transition dipoles make with $\vec{R}$, the vector connecting the two dipoles. τ_R $[s^{-1}]$ is the radiative lifetime of the exciton, c is the speed of light, n is the refractive index of the host medium, and N_A is Avogadro's number $[mol^{-1}]$.

If the exciton population lifetime was arbitrarily large, the scenario for system dynamics in the weak excitation regime would start with absorption of the nonresonant excitation pulse, followed by rapid intradot thermalization, resulting in an initial (tens of picoseconds) distribution of excitons within the ensemble (either monodispersed or bimodal) that closely resembles the distribution of dot sizes (and therefore the solution spectrum at room temperature, with the homogeneous line width deconvolved). Any given dot in the ensemble will be surrounded by dots of different sizes, and if initially populated, would transfer via the Förster interaction to one of the nearby dots. For a given nearest-neighbor separation, the transfer rate would be highest to larger dots if available, whose absorption spectrum best overlaps with the populated dot's emission spectrum. Excitons in larger dots transfer to nearby smaller dots but at a much lower rate for a given separation, depending on temperature. The spectrally windowed TDPL spectra recorded here and in the literature monitor the net effect of scattering in- and scattering-out processes for a given dot size, specified by the emission wavelength. For a specific populated dot, assuming a dilute population of excitons among the dots, the initial scattering out rate is the sum of the transfer rates to adjacent dots. The scattering-in rate to that dot, assuming it is unpopulated, is the sum of the Förster rates from all adjacent, populated dots. Eventually the excitons distribute themselves among the available dots in an approximately Maxwellian (at the temperatures considered here), quasi-thermal distribution where the net scattering-in and scattering-out rates, in an ensemble sense, are equal.

Thus if the quasi-steady state distribution of excitons is similar to the distribution of dots themselves (approximately the case at high temperature in unimodal samples), one would expect little evidence of the Förster transfer processes in the TDPL curves even though Förster mediated interdot transfers are occurring. This is consistent with the observations, as depicted in Figure 2a. When there is a large difference between the quasi-steady state distribution and the distribution of dots (the case at low temperature, especially in bimodal samples), TDPL curves from relatively scarce, relatively small dots at the blue extreme of the spectrum should be dominated by a fast decaying component that reflects the net Förster-mediated scattering-out rate to a distribution of surrounding (larger) dots. This is in general wavelength-dependent and not necessarily monotonic. Spectra from relatively scarce, relatively large dots at the extreme red side of the steady-state spectrum should be dominated by a fast rising signal that reflects the net Förster-mediated scattering-in rate from a distribution of surrounding (smaller) dots. This too will be wavelength dependent and not necessarily monotonic. At intermediate dot sizes, the TDPL curves will exhibit short-term Förster-related transients that are due to a combination of scattering-in and scattering-out rates each to or from a distribution of different sized dots.

■ ANALYSIS

In order to extract representative time constants from the decay curves in Figures 2 and 3 for the different filters and temperatures, they were all fit using

$$y = Ae^{-t/\tau_a} + Be^{-t/\tau_b} + C \quad (3)$$

where the short time constant is associated with the net rate of exciton transfer between dots; it can have either a negative or positive amplitude depending on whether the initially excited

dx.doi.org/10.1021/jp4109046 | J. Phys. Chem. C 2014, 118, 1377−1385

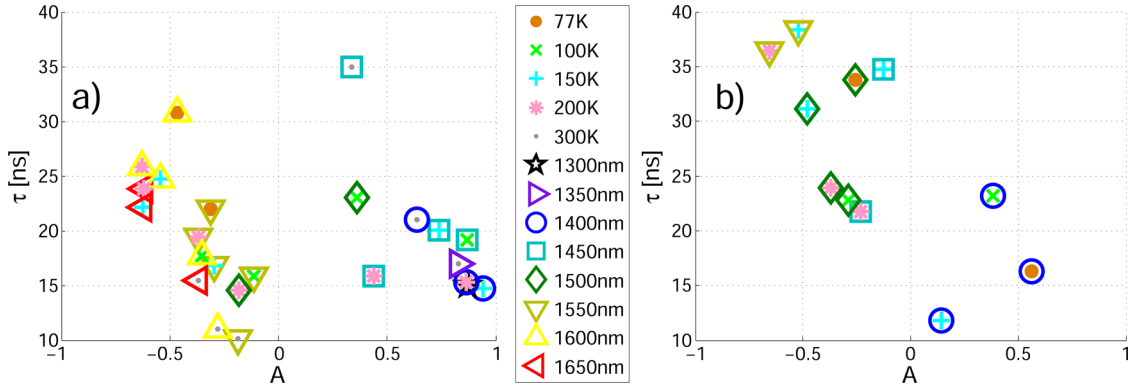

Figure 6. The fast time constants extracted from the TDPL curves using eq 3 as a function of normalized amplitude for the unimodal sample B (a), and the bimodal mixture of A and B (b). The positive amplitude corresponds with fast decay and the negative amplitude with the net buildup time. The scatter in the data points reflects the uncertainty in the parameter estimations.

exciton population is below or above the quasi-steady-state value. The long time constant characterizes the steady state population decay and this term can only have a positive amplitude.

Figure 5a (unimodal drop-cast sample A) and Figure 5b (bimodal drop-cast sample) summarize the extracted time constants from 77 to 300 K, averaged over all of the detected wavelengths for a given sample and a given temperature. Over the entire temperature range and for both sample distributions, the average fast exciton transfer time constants are all well-separated (significantly faster) than the population decay time constants. We note that the spectrally averaged and spectrally integrated population decay times are almost identical for the unimodal and bimodal samples.

In contrast, some wavelength dependence for the fast, Förster-related time constant is expected from eq 2. For extremely small particles, initially populated by the pulsed laser on the high energy side of the distribution, their decay rate will be dominated by scattering out, primarily into larger particles with absorption spectra that best overlap the populated particle's emission spectrum, in proportion to the density of those particles in their surroundings.[21] We argue that it is only this segment of the dot distribution that decay in a way that can be directly related to a relatively simple (at least conceptually) Förster scattering rate calculation, given the more complicated scenario outlined below for larger dots.

For relatively large particles on the red side of the distribution, especially at lower temperatures, their occupation will build up from the initially excited values due to Förster related scattering-in from a range of surrounding particles. Because this in-scattering rate is not proportional to the occupation of the receptor dot, we do not see any "simple" way to directly relate this rate to an intuitive Förster scattering rate calculation. Nevertheless, to a good approximation when the population lifetime is considerably faster than the decay and buildup time constants, the conservation of excitons means that the buildup times must be directly related to the decay times when a full self-consistent analysis is done.

Figure 6 plots the measured fast time constants versus their associated (normalized) amplitudes (the *A* parameter in eq 3). All of the temperatures and wavelengths appear on these "universal plots", one for each of the sample types. Note that there is a very strong correlation between the wavelengths and the magnitudes of the amplitudes; the blue shift for the positive amplitude data increases with amplitude, and the redshift of the negative amplitude data increases with the absolute value of the amplitude. The following discussion is based primarily on the bimodal sample data, which has several representative values from both the blue (positive amplitudes) and red (negative amplitudes) sides of the spectra, in contrast to the monodispersed sample, which has a much narrower emission spectrum compared to our filter center-frequency separation.

From the data in Figure 6, we first conclude that for both sample types, the variation with temperature does not follow any clear trend, and its average value varies little over the whole temperature range in comparison to the variation of the lifetime with wavelength for each temperature (consistent with Figure 5). For the bimodal distribution, the variation with wavelength is on the order of the scatter in the data due to measurement uncertainties but it is sufficient to conclude that there is a definite trend for the fast lifetime to increase on the blue side of the spectra, as the participating dots get larger and approach the mean size, while the lifetime similarly increases on the red side of the spectrum the more the dot size increases away from the mean. Following the discussion above, if we limit an intuitive explanation to the positive amplitude, the blue-shifted portion of the data, then this dependence on wavelength can be used to infer the energy difference between "optimally coupled" donor−acceptor pairs[20] for which the spectral overlap integral in eq 2 is a maximum. An energy difference of less than ∼50 meV would mean that the fast time constant of the most blue shifted of the dots would be associated with scattering out primarily to receptor dots with energies on the blue side of the bimodal density of states (represented by the dashed blue curve in Figure 4a). The time constant should decrease for less blue-shifted dots then remain roughly constant before increasing as the principal receptor dots energy moved to the red side of the roughly flat-toped density of states. An energy difference of more than 100 meV would suggest that the fast time constant would increase monotonically as the blue shift of the donor dots decreased but by more than a factor of 2 times because the density of states falls off rapidly below ∼6500 cm^{-1}. We therefore deduce that the energy separation associated with optimal donor−acceptor exchange is between 50 and 100 meV in these samples. This is consistent with the conclusion reached in ref 20, where PbS nanocrystals were studied.

As mentioned above, we see no simple way to predict or interpret the wavelength variation of the fast buildup time constant with wavelength and/or (correlated) negative amplitude in Figure 6, but it is interesting that the buildup

dx.doi.org/10.1021/jp4109046 | J. Phys. Chem. C 2014, 118, 1377−1385

time in the bimodal sample exhibits a similar variation as the decay time, albeit with a larger range of variation, and a similar mean. On the basis of exciton number conservation at short times, the fact that the mean decay time is very similar to the mean buildup time makes sense. That the negative amplitude time constant data is to some extent a laterally translated version of the positive amplitude time constant data in Figure 6a may be related to the inferred energy separation of between 50 and 100 meV between optimally coupled donors and acceptors but we can not quantify this conjecture.

The relative lack of data for the monodispersed sample makes it difficult to draw strong conclusions about the wavelength dependence of the fast time constant. As indicated in Figure 6, the average values of the fast time constant vary less with temperature than the variation with wavelength, and the scatter in the data.

From this data and analysis, we therefore conclude that the spectrally averaged Förster-related relaxation rate is at most weakly temperature dependent in both the monodispersed and bimodal blend samples over this temperature range. Most significantly, in both samples the variation in the time constant over the spectrum (including both decay and buildup transients) at a fixed temperature exceeds the total variation of the average with temperature and between samples.

The weak temperature dependence of the average Förster time constant observed in both of our samples and in ref 8deserves comment. With reference to eq 2, the net scattering out time from a relatively small dot will be dominated by its transfer rate to slightly larger (more numerous) dots whose absorption spectrum best overlaps with the small dot's emission spectrum. We are unaware of high-quality temperature-dependent emission and absorption data from single quantum dots, however a simple numerical evaluation of this scattering out rate for a given, optimally overlapped donor–acceptor pair, confirms it is essentially independent of T from 300 to 77 K. The same argument holds for the net scattering in rate for relatively large dots in the distribution. More crudely, one might expect that the spectrally averaged Förster rate we deduce from Figures 2 and 3 could be related to the integral in eq 2, using the ensemble absorption and emission spectra. A full set of temperature dependent absorption and emission spectra from an ensemble of CdSe dots[21] suggests that the integral of spectra in eq 2 is in fact only weakly temperature dependent over the range of temperatures considered here. Given a weak temperature dependence of the spectral overlap integral contribution to k, there then remains the temperature dependence of R and τ_R in eq 2. Given the single-peaked nature of the spectra from our samples over the temperature range, and previous kinetic modeling of the temperature dependent spectra from similar samples,[22] we have no reason to believe that the radiative decay rate has a significant temperature dependence. We have no measure of the temperature dependence of the interparticle separation but based on this interpretation it would appear to be weak.

As noted above, the spectrally averaged long time constant corresponding to exciton population decay is almost identical for the monodispersed and bimodal blend samples, and its variation with temperature is more significant (roughly a factor of 5 increase in the decay rate from 77 to 300 K) than that of the fast time constant. Consistent with previous reports, the relative importance or "efficiency" of Förster-mediated population transfer (if taken as the ratio of these two time constants) increases in both of these samples as the temperature decreases. However, Figure 5 clearly shows that most of this increase in efficiency is due to the reduced long-time exciton population decay rate at lower temperatures. On the basis of other work on similar samples,[16,22,23] we attribute this temperature dependence of the long time constant to a reduced nonradiative recombination rate at lower temperatures, owing to its activated nature.

However, it is not clear to what extent the average fast time constant extracted from the TDPL curves is the relevant Förster parameter to include in an efficiency figure of merit. Careful inspection of the temporal evolution of the spectra in Figure 4 suggests that the characteristic time required for the spectra to attain their quasi-steady-state shape is typically between 100 and 200 ns, much longer than the "fast time constant" extracted from the spectrally filtered TDPL curves. Thus in some sense, the net Förster-related equilibration time for the excitons to come within ~10% of their quasi-steady state distribution is more like 150 ns than 20–30 ns. A very simple four level kinetic model captures the essence of this somewhat counterintuitive observation. With reference to Figure 7, if we assume a scattering rate γ_{12} from a donor state 1 to an acceptor state 2, γ_{21} for the reverse scattering rate, and a common γ_r recombination rate for both states 1 and 2 returning to their respective ground states, the corresponding rate equations are

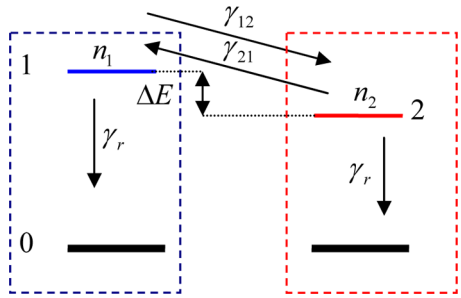

Figure 7. Energy level and scattering rate diagram for a donor (left) and acceptor (right) pair of QDs with resonant transition energies separated by ΔE, and Förster-related scattering rates γ_{21} and γ_{12}. Both populations are assumed to decay at a rate γ_r.

$$\frac{dn_1}{dt} = -(\gamma_r + \gamma_{12})n_1 + \gamma_{21}n_2$$
$$\frac{dn_2}{dt} = \gamma_{21}n_1 - (\gamma_r + \gamma_{21})n_2 \quad (4)$$

The simple donor–acceptor absorption/emission model referred to above confirms that γ_{21} varies as $\exp(-\Delta E/kT)$ over the temperature range of interest here, when ΔE is chosen to maximize the donor–acceptor scattering rate, γ_{12}, which as noted above is essentially temperature independent. This ratio of interstate scattering rates ensures that the quasi-steady-state population ratio in states 1 and 2 is Maxwellian. Solving the set of eqs 4, assuming some arbitrarily initial populations $n_1(t = 0) = N_1$ and $n_2(t = 0) = N_2$ yields transient solutions

dx.doi.org/10.1021/jp4109046 | J. Phys. Chem. C 2014, 118, 1377–1385

$$n_1(t) = \left(\frac{\gamma_{12}N_1 - \gamma_{21}N_2}{\gamma_{12} + \gamma_{21}}\right)\exp(-\Gamma_1 t) + \left(\frac{\gamma_{21}N_1 + \gamma_{21}N_2}{\gamma_{12} + \gamma_{21}}\right)\exp(-\Gamma_2 t)$$

$$n_2(t) = \left(\frac{-\gamma_{12}N_1 + \gamma_{21}N_2}{\gamma_{12} + \gamma_{21}}\right)\exp(-\Gamma_1 t) + \left(\frac{\gamma_{12}N_1 + \gamma_{12}N_2}{\gamma_{12} + \gamma_{21}}\right)\exp(-\Gamma_2 t) \quad (5)$$

where

$$\Gamma_1 = \gamma_{12} + \gamma_{21} + \gamma_r$$

$$\Gamma_2 = \gamma_r$$

One state population decays and another increases so that their ratio approaches the quasi-equilibrium value with a fast time constant equal to the sum of the three relevant time constants. In the experimentally relevant case where $\gamma_r \ll \gamma_{12}$ eq 5 shows that the short-time response is approximately

$$n_1(t) = n_{1ss} + (N_1 - n_{1ss})\exp(-\Gamma_1 t)$$

$$n_2(t) = n_{2ss} + (N_2 - n_{2ss})\exp(-\Gamma_1 t) \quad (6)$$

where

$$n_{1ss} = \frac{(N_1 + N_2)}{\left(1 + \exp\left(\frac{\Delta E}{kT}\right)\right)}$$

$$n_{2ss} = (N_1 + N_2) - n_{1ss} \quad (7)$$

The relevant quantity to assess the extent to which the spectra (populations) have reached quasi-equilibrium is the ratio, $n_1(t)/n_2(t)$, which clearly does not vary exponentially. One cannot therefore ascribe a clear "time constant" for this equilibration process, but inserting parameters consistent with those in Figures 5 and 7 (γ_{12} = 1/20 ns, γ_r = 1/500 ns, and γ_{21} = 1/500 ns), we find that the $n_1(t)/n_2(t)$ ratio comes within 10% of its quasi-equilibrium value in ~150 ns, completely consistent with the time observed in the set of spectra within Figure 4.

CONCLUSIONS

A detailed analysis of the spectral and temperature dependence of the steady-state and time-resolved photoluminescence spectra from both unimodal and bimodal solid state emulsions of PbSe quantum dots emitting in the infrared near 7000 cm^{-1} indicates that (i) the average of the fast transient decay times observed on the blue side of the spectra and the fast transient buildup times observed on the red side of the spectra is essentially independent of temperature, ~20−25 ns from 77 to 300 K, (ii) the variation of the this fast transient time constant at a fixed temperature, as a function of wavelength is considerable (from 10 to 40 ns) and at least qualitatively consistent with what is predicted from the theoretical expression for the Förster transfer rate where the optimal overlap of the donor emission and acceptor absorption spectra occurs for an energy separation of between 50 and 100 meV, and (iii) the population lifetime of the QDs is the same for all dots in the emulsions, and it increases by a factor of ~5 times from 300 to 77 K. If one uses the fast time constant as a measure of the Förster interaction rate, the "Förster efficiency", intended as a measure of how much exciton migration among the QD ensemble occurs before they decay, thus changes by a factor of 5 times between 300 and 77 K but this is entirely due to the temperature dependence of the population lifetime. The temperature independence of the Förster rate is consistent with modeling the theoretical expression for the coupling rate between optimally separated donor−acceptor pairs and also with the temperature dependence of absorption and emission spectra from QD ensembles in the literature over this temperature range. Finally, we note that the fast time constant extracted from spectrally resolved decay and buildup transients is at least five times shorter than the (nonexponential) time it takes for the exciton population to approach within ~10% of its quasi-steady state shape (consistent with a simple model), which suggests that the typically used "Förster efficiency" is ambiguous and at best a qualitative measure of the degree to which the excitons equilibrate before decaying.

AUTHOR INFORMATION

Corresponding Author

*E-mail: rquintero@fata.unam.mx.

Notes

The authors declare no competing financial interest.

ACKNOWLEDGMENTS

We gratefully acknowledge the assistance of Charles Foell, Keith Abel, and Jothir Mayanantham in preparing the samples and useful discussions with Russ Algar. The financial assistance of the Natural Sciences and Engineering Research Council of Canada, and the Canadian Institute for Advanced Research is also acknowledged. R.Q.T. acknowledges the financial assistance of DGAPA, UNAM.

REFERENCES

(1) Kongkanand, A.; Tvrdy, K.; Takechi, K.; Kuno, M.; Kamat, P. V. Quantum Dot Solar Cells. Tuning Photoresponse Through Size and Shape Control of CdSe-TiO_2 Architecture. *J. Am. Chem. Soc.* **2008**, *130*, 4007−4015.

(2) Szendrei, K.; Speirs, M.; Gomulya, W.; Jarzab, D.; Manca, M.; Mikhnenko, O. V.; Yarema, M.; Kooi, B. J.; Heiss, W.; Loi, M. A. Exploring the Origin of the Temperature-Dependent Behavior of PbS Nanocrystal Thin Films and Solar Cells. *Adv. Funct. Mater.* **2012**, *22*, 1598−1605.

(3) Sukhovatkin, V.; Hinds, S.; Brzozowski, L.; Sargent, E. H. Colloidal Quantum-Dot Photodetectors Exploiting Multiexciton Generation. *Science* **2009**, *324*, 1542−1544.

(4) Konstantatos, G.; Sargent, E. H. Nanostructured Materials for Photon Detection. *Nat. Nanotechnol.* **2010**, *5*, 391−400.

(5) Talapin, D. V.; Lee, J. S.; Kovalenko, M. V.; Shevchenko, E. V. Prospects of Colloidal Nanocrystals for Electronic and Optoelectronic Applications. *Chem. Rev.* **2010**, *110*, 389−458.

(6) Knox, R. S.; van Amerongen, H. Refractive Index Dependence of the Forster Resonance Excitation Transfer Rate. *J. Phys. Chem. B* **2002**, *106*, 5289−5293.

(7) Parson, W. W. *Modern Optical Spectroscopy*; Springer-Verlag: Berlin, 2007; pp 259−280.

(8) Shi, L. F.; De Paoli, V.; Rosenzweig, N.; Rosenzweig, Z. Synthesis and Application of Quantum Dots FRET-Based Protease Sensors. *J. Am. Chem. Soc.* **2006**, *128*, 10378−10379.

(9) Lunz, M.; Bradley, A. L.; Gerard, V. A.; Byrne, S. J.; Gun'ko, Y. K.; Lesnyak, V.; Gaponik, N. Concentration Dependence of Forster Resonant Energy Transfer Between Donor and Acceptor Nanocrystal Quantum Dot Layers: Effect of Donor-Donor Interactions. *Phys. Rev. B: Condens. Matter.* **2011**, *83*, 115423.

(10) Clark, S. W.; Harbold, J. M.; Wise, F. W. Resonant Energy Transfer In PbS Quantum Dots. *J. Phys. Chem C* **2007**, *111*, 7302−7305.

(11) Clapp, A. R.; Medintz, I. L.; Mattoussi, H. Forster Resonance Energy Transfer Investigations Using Quantum-Dot Fluorophores. *ChemPhysChem* **2006**, *7*, 47−57.
(12) Crooker, S. A.; Hollingsworth, J. A.; Tretiak, S.; Klimov, V. I. Spectrally Resolved Dynamics of Energy Transfer in Quantum-Dot Assemblies: Towards Engineered Energy Flows in Artificial Materials. *Phys. Rev. Lett.* **2002**, *89*, 186802.
(13) Gao, Y. N.; Talgorn, E.; Aerts, M.; Trinh, M. T.; Schins, J. M.; Houtepen, A. J.; Siebbeles, L. D. A. Enhanced Hot-Carrier Cooling and Ultrafast Spectral Diffusion in Strongly Coupled PbSe Quantum-Dot Solids. *Nano Lett.* **2011**, *11*, 5471−5476.
(14) Lu, W.; Kamiya, I.; Ichida, M.; Ando, H. Temperature Dependence of Electronic Energy Transfer in PbS Quantum Dot Films. *Appl. Phys. Lett.* **2009**, *95*, 83102.
(15) Wuister, S. F.; Koole, R.; Donega, C. D.; Meijerink, A. Temperature-Dependent Energy Transfer in Cadmium Telluride Quantum Dot Solids. *J. Phys. Chem B* **2005**, *109*, 5504−5508.
(16) Abel, K. A.; Qiao, H. J.; Young, J. F.; van Veggel, F. C. J. M. Four-Fold Enhancement of the Activation Energy for Nonradiative Decay of Excitons in PbSe/CdSe Core/Shell versus PbSe Colloidal Quantum Dots. *J. Phys. Chem. Lett.* **2010**, *1*, 2334−2338.
(17) Murray, C. B.; Sun, S. H.; Gaschler, W.; Doyle, H.; Betley, T. A.; Kagan, C. R. Colloidal Synthesis of Nanocrystals and Nanocrystal Superlattices. *IBM J. Res. Dev.* **2001**, *45*, 47−56.
(18) Stouwdam, J. W.; Shan, J.; van Veggel, F. C. J. M.; Pattantyus-Abraham, A. G.; Young, J. F.; Raudsepp, M. Photostability of Colloidal PbSe And PbSe/PbS Core/Shell Nanocrystals in Solution and in the Solid State. *J. Phys. Chem C* **2007**, *111*, 1086−1092.
(19) Abel, K. A.; FitzGerald, P. A.; Wang, T. Y.; Regier, T. Z.; Raudsepp, M.; Ringer, S. P.; Warr, G. G.; van Veggel, F. C. J. M. Probing the Structure of Colloidal Core/Shell Quantum Dots Formed by Cation Exchange. *J. Phys. Chem C* **2012**, *116*, 3968−3978.
(20) Bose, R.; McMillan, J. F.; Gao, J.; Rickey, K. M.; Chen, C. J.; Talapin, D. V.; Murray, C. B.; Wong, C. W. Temperature-Tuning of Near-Infrared Monodisperse Quantum Dot Solids at 1.5 Mu M For Controllable Forster Energy Transfer. *Nano Lett.* **2008**, *8*, 2006−2011.
(21) Chi, T. T. K.; Thuy, U. T. D.; Liem, N. Q.; Nam, M. H.; Thanh, D. X. Temperature-Dependent Photoluminescence and Absoprtion of CdSe Quantum Dots Embedded in PMMA. *J. Korean Phys. Soc.* **2008**, *52*, 1510−1513.
(22) Qiao, H. J.; Abel, K. A.; van Veggel, F. C. J. M.; Young, J. F. Exciton Thermalization and State Broadening Contributions to the Photoluminescence of Colloidal PbSe Quantum Dot Films From 295 to 4.5 K. *Phys. Rev. B: Condens. Matter.* **2010**, *82*, 161414.
(23) Quintero-Torres, R.; Foell, C. A.; Pichaandi, J.; van Veggel, F. C. J. M.; Young, J. F. Photoluminescence Dynamics in Solid Formulations of Colloidal PbSe Quantum Dots: Three-Dimensional Versus Two-Dimensional Films. *Appl. Phys. Lett.* **2012**, *101*, 121904.